数理解析研究所講究録
第1543巻 2007年 76-85

A Set of Equations for Strongly Nonlinear and Strongly Dispersive Surface/Internal Waves

港湾空港技術研究所　海洋・水工部　柿沼　太郎（Taro Kakinuma）
Marine Environment and Engineering Dept.,
Port and Airport Research Institute

1. INTRODUCTION

In a lake or the ocean where density stratification is well developed, not only internal long-period waves, e.g. internal seiches and tides, but also internal short-period waves can be observed;[1] the sources of the latter include bottom topography and interfacial instability. Such internal waves exchange their energy among components over a wide wave-frequency band, with strong nonlinearity especially when they reach shallow water regions.

The nonlinearity and dispersivity of internal waves, however, have been closely studied for only internal long waves, where internal-long-wave equations were derived to evaluate interface profiles without disturbance or mixing due to numerical errors. For example, on a perturbation basis, Matsuno[2] proposed internal-wave equations for arbitrary aspect ratios with *weak nonlinearity* and *strong dispersivity*. Choi and Camassa[3] derived two sets of internal-wave equations considering *full nonlinearity* of internal waves in a two-layer system, where we choose one set of equations to treat a shallow layer whether it lies on another shallow layer with *weak dispersivity* or a deep layer with *intermediate dispersivity*. The horizontally two-dimensional resonance of internal solitons are numerically simulated by Tsuji and Oikawa[4] with *mild dependence* on motion in the direction of y-axis, as well as *weak nonlinearity* and *weak dispersivity*.

On the other hand, Kakinuma[5] did not use any assumption on nonlinearity, as well as dispersivity, of internal waves in the derivation process of a set of nonlinear internal-wave equations based on a *three-dimensional* variational principle of multilayer-fluid motion. For this reason the application of this model is theoretically free from limitations concerning the relative thickness of fluid layers or the frequency band of *strongly nonlinear* and *strongly dispersive* surface/internal waves. In the present paper, several numerical results of this set of equations are shown for internal waves of a two-layer system in the vertically two-dimensional plane.

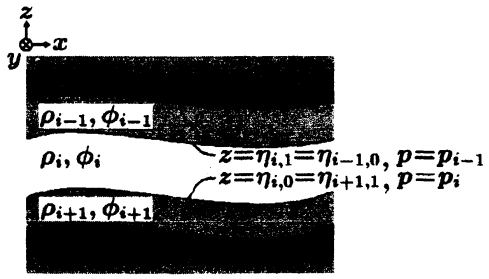

Fig. 1 Multilayer fluid system.

2. FULLY NONLINEAR EQUATIONS FOR SURFACE/INTERNAL WAVES

2.1 Multilayer fluids

Inviscid and incompressible fluids are assumed to be stable in still water, as shown in **Fig. 1**, where these fluids are represented as i (i = 1, 2, $\cdots$, I) from top to bottom. The i-layer thickness in still water is denoted by $h_i(\boldsymbol{x})$. None of the fluids mix even with motion. The density ρ_i is spatially uniform and temporally constant in each layer, where $\rho_1 < \rho_2 < \cdots < \rho_I$. Surface tension and capillary action are neglected.

Fluid motion is assumed to be irrotational, resulting in the existence of velocity potential ϕ_i defined as

$$\boldsymbol{u}_i = \nabla\phi_i \quad \text{and} \quad w_i = \partial\phi_i/\partial z, \tag{1}$$

where ∇ is a partial differential operator in the horizontal plane, i.e., $\nabla = (\partial/\partial x, \partial/\partial y)$.

2.2 Functional for the variational problem

The pressure on $z = \eta_{i,0}$, i.e., the lower interface of the i-layer, is written by $p_i(\boldsymbol{x}, t)$. In the i-layer, if both the elevation of one interface, $z = \eta_{i,1-j}(\boldsymbol{x}, t)$ (j = 0 or 1), and the pressure on the other interface, $p_{i-j}(\boldsymbol{x}, t)$, are known, then the unknown variables are the velocity potential $\phi_i(\boldsymbol{x}, z, t)$ and interface elevation $\eta_{i,j}(\boldsymbol{x}, t)$ such that the functional for the variational problem in the i-layer, F_i, is determined by

$$F_i[\phi_i, \eta_{i,j}] = \int_{t_0}^{t_1} \iint_A \int_{\eta_{i,0}}^{\eta_{i,1}} \left\{ \frac{\partial\phi_i}{\partial t} + \frac{1}{2}(\nabla\phi_i)^2 + \frac{1}{2}\left(\frac{\partial\phi_i}{\partial z}\right)^2 + gz + \frac{p_{i-j} + P_i}{\rho_i} \right\} dz\, dA\, dt, \tag{2}$$

where $P_i = \sum_{k=1}^{i-1}(\rho_i - \rho_k) g h_k$; g is gravitational acceleration; the plane A, which is the orthogonal projection of the object domain onto the x-y plane, is assumed to be independent of time.

In comparison with the functional referred to in Luke[6] for rotational

motion, Eq. (2) has an additional term of the interfacial pressure without the terms relating to vorticity.

2.3 Vertically distributed functions

In order to derive a set of equations whose type is horizontally two-dimensional, vertical integration is performed analytically. In a manner similar to that for the fully nonlinear surface-wave model,[7] the velocity potential ϕ_i is expanded into a series in terms of a given set of vertically distributed functions $Z_{i,\alpha}$ multiplied by their weightings $f_{i,\alpha}$, i.e.,

$$\phi_i(x,z,t)=\sum_{\alpha=0}^{N-1} Z_{i,\alpha}(z,h_i(x))f_{i,\alpha}(x,t)\equiv Z_{i,\alpha}f_{i,\alpha}, \tag{3}$$

where N is the number of vertically distributed functions and the sum rule of product is adopted for subscript α.

2.4 Euler-Lagrange equations under variational principle

We substitute Eq. (3) into Eq. (2), after which the functional F_i is integrated vertically. Then the variational principle is applied to obtain the following Euler-Lagrange equations, i.e., the fully nonlinear equations for surface and internal waves:[5]

$$Z_{i,\alpha}^{\eta_{i,1}}\frac{\partial\eta_{i,1}}{\partial t}-Z_{i,\alpha}^{\eta_{i,0}}\frac{\partial\eta_{i,0}}{\partial t}+\nabla\left(\int_{\eta_{i,0}}^{\eta_{i,1}}Z_{i,\alpha}Z_{i,\beta}\,dz\,\nabla f_{i,\beta}\right)-\int_{\eta_{i,0}}^{\eta_{i,1}}\frac{\partial Z_{i,\alpha}}{\partial z}\frac{\partial Z_{i,\beta}}{\partial z}dz f_{i,\beta}=0, \tag{4}$$

$$Z_{i,\beta}^{\eta_{i,j}}\frac{\partial f_{i,\beta}}{\partial t}+\frac{1}{2}Z_{i,\beta}^{\eta_{i,j}}Z_{i,\gamma}^{\eta_{i,j}}\nabla f_{i,\beta}\nabla f_{i,\gamma}+\frac{1}{2}\frac{\partial Z_{i,\beta}^{\eta_{i,j}}}{\partial z}\frac{\partial Z_{i,\gamma}^{\eta_{i,j}}}{\partial z}f_{i,\beta}f_{i,\gamma}+g\eta_{i,j}+\frac{p_{i-j}+P_i}{\rho_i}=0, \tag{5}$$

where $\alpha = 0, 1, 2, \cdots, N-1$; $Z_{i,\alpha}^{\eta_{i,e}} \equiv Z_{i,\alpha}\big|_{z=\eta_{i,e}}$ ($e = 0$ or 1); $\partial Z_{i,\alpha}^{\eta_{i,j}}/\partial z \equiv \partial Z_{i,\alpha}/\partial z\big|_{z=\eta_{i,j}}$.

3. Two-layer problems between horizontal plates

3.1 Nonlinear two-layer equations

We consider two-layer problems between two fixed horizontal plates, where $\eta_{1,1} = 0$ and $\eta_{2,0} = -(h_1+h_2) \equiv -D$. The set of nonlinear equations for surface/internal waves are reduced to a set of nonlinear two-layer equations, after which several numerical results are shown for interface displacements and horizontal velocities.

The interface profile is described by $z = \eta\,(x, t)$, where $\eta = \eta_{1,0} = \eta_{2,1}$. In this paper the vertically distributed function $Z_{i,\alpha}$ is determined by

$$Z_{i,\alpha}=\left\{\left(z+\sum_{k=0}^{i-j}h_k\right)/h_i\right\}^{\alpha}. \tag{6}$$

[1-layer]

In the 1-layer, i.e., the upper layer, $i = 1$ and $j = 0$. We introduce ζ defined as

$$\zeta=\frac{\eta+h_1}{h_1}, \tag{7}$$

after which Eq. (6) is substituted into Eqs. (4) and (5), resulting in

$$\zeta^{\alpha}\frac{\partial\zeta}{\partial t}+\frac{1}{\alpha+\beta+1}\nabla\left\{\left(\zeta^{\alpha+\beta+1}-1\right)\nabla f_{1,\beta}\right\}-\frac{1}{h_1^{\,2}}\frac{\alpha\beta}{\alpha+\beta-1}\left(\zeta^{\alpha+\beta-1}-1\right)f_{1,\beta}=0, \tag{8}$$

$$\zeta^{\beta}\frac{\partial f_{1,\beta}}{\partial t}+\frac{1}{2}\zeta^{\beta+\gamma}\nabla f_{1,\beta}\nabla f_{1,\gamma}+\frac{1}{2}\frac{\beta\gamma}{h_1^{\,2}}\zeta^{\beta+\gamma-2}f_{1,\beta}f_{1,\gamma}+g\eta+\frac{p_1}{\rho_1}=0. \tag{9}$$

[2-layer]

In the 2-layer, i.e., the lower layer, $i = 2$ and $j = 1$. We introduce ξ defined as

$$\xi=\frac{\eta+h_1}{h_2}, \tag{10}$$

after which Eq. (6) is substituted into Eqs. (4) and (5), leading to

$$\begin{aligned}\xi^{\alpha}\frac{\partial\xi}{\partial t}&+\frac{1}{\alpha+\beta+1}\nabla\left\{\left[\xi^{\alpha+\beta+1}-(-1)^{\alpha+\beta+1}\right]\nabla f_{2,\beta}\right\}\\&-\frac{1}{h_2^{\,2}}\frac{\alpha\beta}{\alpha+\beta-1}\left\{\xi^{\alpha+\beta-1}-(-1)^{\alpha+\beta-1}\right\}f_{2,\beta}=0,\end{aligned} \tag{11}$$

$$\begin{aligned}\xi^{\beta}\frac{\partial f_{2,\beta}}{\partial t}&+\frac{1}{2}\xi^{\beta+\gamma}\nabla f_{2,\beta}\nabla f_{2,\gamma}+\frac{1}{2}\frac{\beta\gamma}{h_2^{\,2}}\xi^{\beta+\gamma-2}f_{2,\beta}f_{2,\gamma}\\&+g\eta+\frac{p_1+(\rho_2-\rho_1)gh_1}{\rho_2}=0.\end{aligned} \tag{12}$$

Eqs. (8), (9), (11), and (12) can be solved using a finite difference method presented by Kakinuma and Nakayama[8], the results of which are shown in the following subsections.

3.2 Numerical simulation of long waves

Two-layer problems are solved in vertically two-dimensional cases. Horn *et*

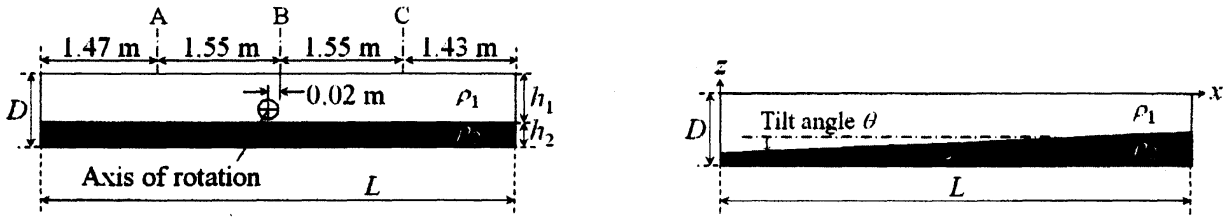

(a) Dimensions of the laboratory tank.[9)]

(b) Initial condition of calculation. The interface is inclined with the angle θ in the horizontal tank.

Fig. 2 Schematic of tanks.

al.[9)] performed hydraulic experiments using a tank, whose length L, depth D, and width W were 6.0 m, 0.29 m, and 0.3 m, respectively, as shown in **Fig. 2(a)**. Three ultra-sonic wave gauges were set at the positions marked A, B, and C. This tank was filled with a two-layer stratification, where $h_1/D = 0.8$, after which it was rotated very slowly through θ around the axis of rotation. At the beginning of the experiments, this tilted tank was returned to a horizontal position very quickly. In the initial condition of numerical computations, the tank is horizontal and the interface is inclined linearly as shown in **Fig. 2(b)**.

The grid width Δx and time-step interval Δt are equal to 0.06 m and 0.02 s, respectively, throughout every computation performed in the present study.

In **Figs. 3 – 5**, the experimental and calculation results are compared for the time series of interface displacements at the position marked C in **Fig. 2(a)**, where the density ratio ρ_2/ρ_1 and the tilt angle θ are equal to 1.019 and 0.4617°, respectively. **Fig. 3** shows the experimental result measured by the wave gauge at position C. **Fig. 4** shows the corresponding calculation result through a Boussinesq-type model[10)] (BT), whose fundamental equations are written in **APPENDIX**. **Fig. 5** shows the calculation results obtained using the proposed fully nonlinear model (FN) including the cases where the number of vertically distributed functions for velocity potential, N, is equal to 1, 2, 3, 4, and 5.

When $N = 1$, the set of fully nonlinear internal-wave equations, i.e., Eqs. (8), (9), (11), and (12), reduces to a set of nonlinear and non-dispersive internal-wave equations, which shows extreme disintegration around the wave crests as shown in **Fig. 5**, without dispersivity balancing with non-linearity.

When $N = 2$, the FN takes into account linear and uniform distributions of u_i and w_i in the direction of z, respectively, such that the balance between the nonlinearity and dispersivity is considered, leading to the more accurate result than that when $N = 1$.

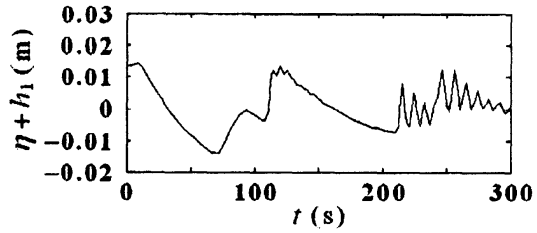

Fig. 3 Time series of interface displacement measured by the wave gauge at position C in the hydraulic experiment.

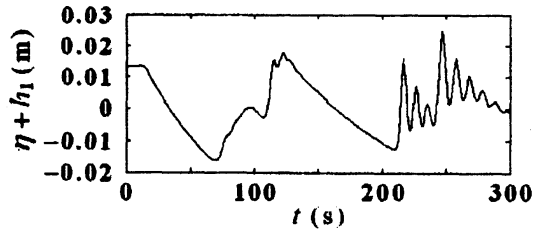

Fig. 4 Time series of interface displacement obtained by the Boussinesq-type model corresponding to that in **Fig. 3**.

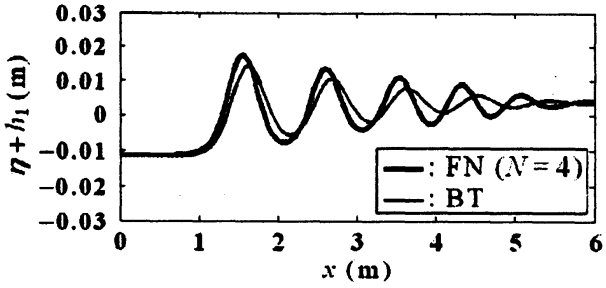

Fig. 6 Interface profiles obtained by the present nonlinear model, where N = 4, and the Boussinesq-type model when t = 280 s.

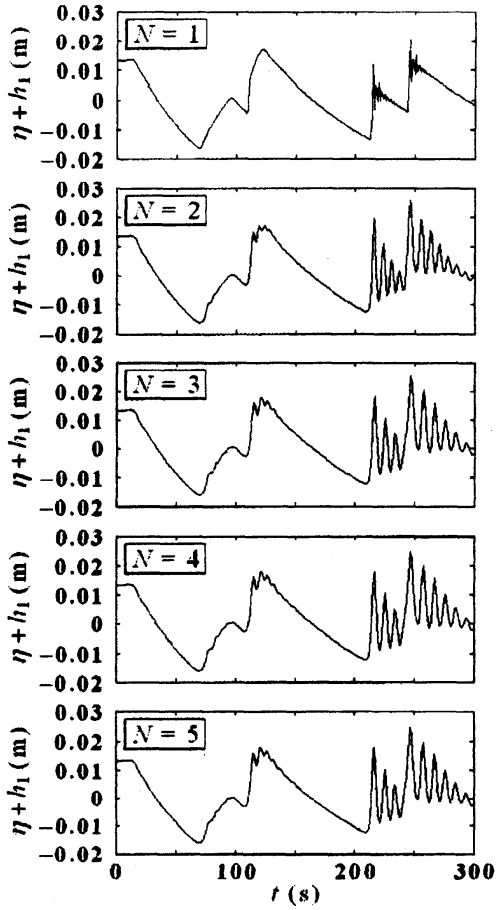

Fig. 5 Time series of interface displacements obtained by the present nonlinear model corresponding to that in **Fig. 3**. The results are shown for different numbers of vertically distributed functions in velocity potential, N.

When N = 3, the interface displacement evaluated by the FN is closer to that in **Fig. 4** obtained by the BT, where the parabolic distribution of u_i in the direction of z is considered in both the FN and BT. It should be noted that though the effect due to the linear distribution of w_i in the direction of z is considered both in the FN and BT, the FN estimates the wave period, or the wave number, more accurately by solving the contribution of each order without perturbation, while the wave period through the BT is longer than that of the experimental data.

The interface displacements obtained by the FN hardly show difference between the cases where N = 4 and 5. Although both the FN and BT do not

include dissipation effects due to friction, which results to larger wave heights than the experimental data, the harmony of results between the FN and BT indicates the high accuracy of results calculated by the FN in this long-wave condition. The interface profiles obtained using the FN, where N = 4, and the BT when t = 280 s are shown in **Fig. 6**, according to which the aspect ratio, i.e., the representative ratio of water depth to wavelength, h_2/λ, is about 0.06. The FN estimates the wave heights larger and the wavelengths shorter with higher nonlinearity than the BT.

3.3 Numerical simulation of intermediate waves

A deeper case, where the representative ratio h_2/λ is around 0.3, is treated in numerical computations. The length L and depth D of the tank shown in **Fig. 2(b)** are 3.0 m and 1.5 m, respectively. The density ratio ρ_2/ρ_1 is 1.02, while the still water depth ratio h_1/D is 0.8 also in this case. In the initial condition of calculation, the tilt angle θ is equal to 5.0°.

Figs. 7 and **8** show the time series of interface displacements at the center of the tank, the former of which was obtained using the BT, while the latter was evaluated by the FN when N = 1, 2, 3, or 4. In this intermediate-wave case, the results show much difference between the BT and FN, which suggests that the BT is not applicable because the set of Boussinesq-type equations was derived on the basis of a perturbation around the long-wave condition with only weak dispersivity, as well as weak nonlinearity.

When N = 1, see **Fig. 8**, the internal waves of the FN show forward leans of their wave profiles, which are restrained when N is larger than one.

It should be noted that even when N = 1 or 2, the FN evaluates the internal-wave periods shorter than those calculated by the BT, which estimates the wave period longer than that of the actual intermediate waves as if the internal waves were long waves.

Fig. 9 shows the vertical distributions of horizontal velocity u_2 in the lower layer below an internal-wave crest, where x = 1.6 m when t = 20 s. The result was obtained using the FN when N = 4 and drawn in the figure for each case where the components up to 0, 1, 2, or 3 of α are added together. Although below the internal-wave crest the difference between u_2's on the interface and bottom is about 5.0 % of u_2 on the bottom, the difference could be important to evaluate internal-wave profiles accurately considering the dispersivity of intermediate waves.

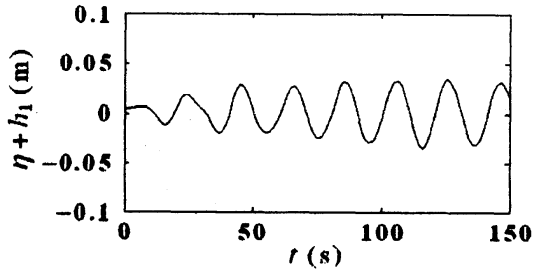

Fig. 7 Time series of interface displacement obtained by the Boussinesq-type model for the intermediate-waves.

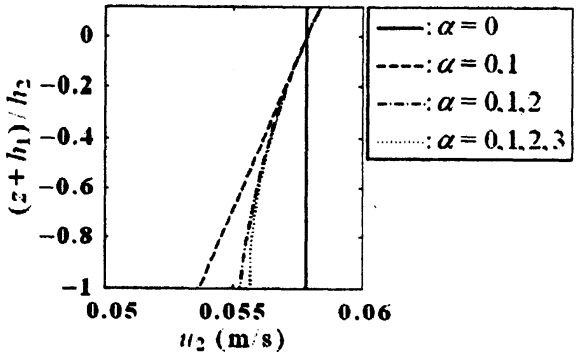

Fig. 9 Vertical distributions of horizontal velocity in the lower layer, u_2, where x = 1.6 m when t = 20 s. The result was obtained using the present nonlinear model when N = 4. Each line shows the velocity distribution where the components are added together up to 0, 1, 2, or 3 of α.

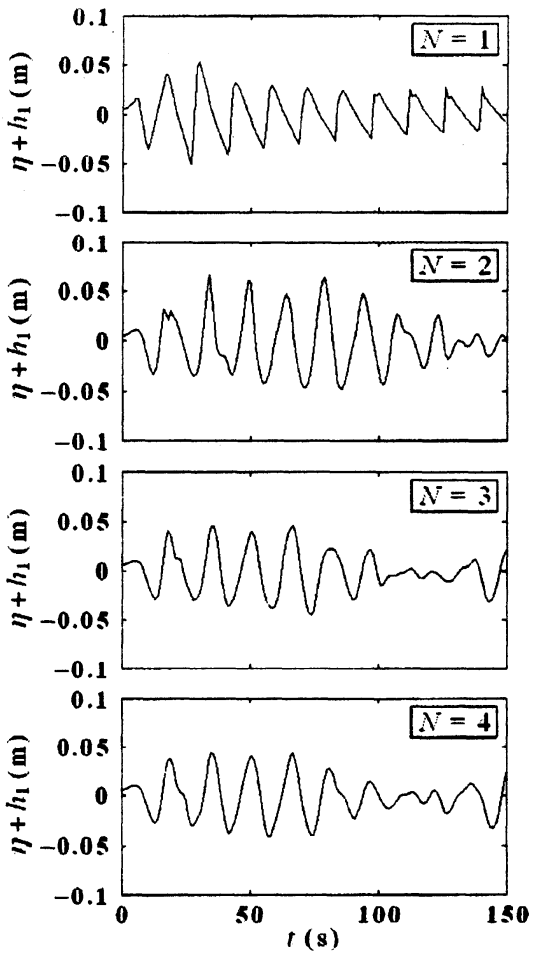

Fig. 8 Time series of interface displacements obtained by the present nonlinear model corresponding to that in **Fig. 7**. The results are shown for different numbers of vertically distributed functions in velocity potential, N.

4. CONCLUSIONS

The internal waves in a two-layer system have been simulated using the set of fully nonlinear internal-wave equations. The computational results of interface displacements up to each order on the vertical length scale of motion were compared with the corresponding calculation results obtained using the Boussinesq-type internal-wave model or the existing experimental data.

In the long-wave case, the interface displacements estimated by the proposed model with more than three vertically distributed functions of

velocity potential were in harmony with that through the Boussinesq-type model, as well as the experimental result especially in the wave number.

In the intermediate-wave case, the proposed model showed different results from those by the Boussinesq-type model, which should not be applied to this case without enough consideration of wave dispersivity.

In computations using the proposed fully nonlinear model with enough number of vertically distributed functions of velocity potential, the weightings of components are evaluated based on the variational principle without assumptions on nonlinearity and dispersivity of waves, such that this model is expected to be applied to multilayer systems including waves of various frequencies over topographies to investigate, for example, generation mechanisms of internal short-period waves from long-period waves such as surface/internal tides.

ACKNOWLEDGMENTS

Sincere gratitude is extended to Dr. Keisuke Nakayama, National Institute for Land and Infrastructure Management, for his cooperation in numerical calculation.

APPENDIX BOUSSINESQ-TYPE EQUATIONS FOR INTERNAL WAVES

The Boussinesq-type equations, several results of which have been shown in this paper, are

[1-layer]

$$\frac{\partial \zeta}{\partial t} + \nabla\{(\zeta - 1)\nabla\phi_1\} = 0, \tag{13}$$

$$\frac{\partial \phi_1}{\partial t} + \frac{1}{2}(\nabla\phi_1)^2 - \frac{1}{3}h_1^2\frac{\partial^3\phi_1}{\partial t\,\partial x^2} + g\eta + \frac{p_1}{\rho_1} = 0, \tag{14}$$

[2-layer]

$$\frac{\partial \xi}{\partial t} + \nabla\{(\xi + 1)\nabla\phi_2\} = 0, \tag{15}$$

$$\frac{\partial \phi_2}{\partial t} + \frac{1}{2}(\nabla\phi_2)^2 - \frac{1}{3}h_2^2\frac{\partial^3\phi_2}{\partial t\,\partial x^2} + g\eta + \frac{p_1 + (\rho_2 - \rho_1)gh_1}{\rho_2} = 0, \tag{16}$$

where ϕ_1 and ϕ_2 are velocity potentials in the upper and lower layers, respectively.

REFERENCES

1) Roberts, J.: Internal Gravity Waves in the Ocean, Marine Science (ed. Hood, D. W.), Marcel Dekker, Inc., Vol. 2, pp. 1-51, 1975.

2) Matsuno, Y.: A unified theory of nonlinear wave propagation in two-layer fluid systems, *J. Phys. Soc. Jpn.*, Vol. 62, pp. 1902-1916, 1993.

3) Choi, W. and Camassa, R.: Fully nonlinear internal waves in a two-fluid system, *J. Fluid Mech.*, Vol. 396, pp. 1-36, 1999.

4) Tsuji, H. and Oikawa, M.: Two-dimensional interaction of solitary waves in a modified Kadomtsev-Petviashvili equation, *J. Phys. Soc. Jpn.*, Vol. 73, pp. 3034-3043, 2004.

5) Kakinuma, T.: A set of fully nonlinear equations for surface and internal gravity waves, *Proc. of the 5th Int. Conf. on Computer Modelling of Seas and Coastal Regions*, WIT Press, pp. 225-234, 2001.

6) Luke, J. C.: A variational principle for a fluid with a free surface, *J. Fluid Mech.*, Vol. 27, pp. 395-397, 1967.

7) Isobe, M.: Time-dependent mild-slope equations for random waves, *Proc. of the 24th Int. Conf. on Coastal Eng.*, ASCE, pp. 285-299, 1995.

8) Kakinuma, T. and Nakayama, K.: Numerical simulation of internal waves using a set of fully nonlinear internal-wave equations, *Annual J. Hydraulic Eng.*, JSCE, Vol.51, CD-ROM, 2007.

9) Horn, D. A., Redekopp, L. G., Imberger, J., and Ivey, G. N.: Internal wave evolution in a space-time varying field, *J. Fluid Mech.*, Vol. 424, pp. 279-301, 2000.

10) Nakayama, K. and Imberger, J.: Residual circulation due to internal waves shoaling on a slope, *J. Phys. Oceanogr.* (in revision)